Article

Porphyrins Fused with Strongly Electron Donating 1,3-Dithole-2-ylidene Moieties. Redox Control by Metal Cation Complexation and Anion Binding

Nathan L. Bill, Masatoshi Ishida, Steffen Bähring, Jong Min Lim, Sangsu Lee, Christina M. Davis, Vincent M. Lynch, Kent Albin Nielsen, Jan O. Jeppesen, Kei Ohkubo, Shunichi Fukuzumi, Dongho Kim, and Jonathan L. Sessler

J. Am. Chem. Soc., **Just Accepted Manuscript** • DOI: 10.1021/ja404830y • Publication Date (Web): 21 Jun 2013

Porphyrins Fused with Strongly Electron Donating 1,3-Dithiol-2-ylidene Moieties. Redox Control by Metal Cation Complexation and Anion Binding

Nathan L. Bill,[a] Masatoshi Ishida,[b] Steffen Bähring,[c] Jong Min Lim,[b] Sangsu Lee,[b] Christina M. Davis,[a] Vincent M. Lynch,[a] Kent A. Nielsen,[c] Jan O. Jeppesen,[c] Kei Ohkubo,[d] Shunichi Fukuzumi,[d,e*] Dongho Kim,[b*] and Jonathan L. Sessler[a,b*]

[a] Department of Chemistry and Biochemistry, University Station-A5300, The University of Texas at Austin, Austin, Texas 78712

[b] Department of Chemistry, Yonsei University, Seoul, 120-750, Korea

[c] Department of Chemistry, Physics, and Pharmacy, University of Southern Denmark, Denmark

[d] Department of Material and Life Science, Graduate School of Engineering, Osaka University, ALCA, Japan Science and Technology Agency, Suita, Osaka 565-0871, Japan

[e] Department of Bioinspired Science, Ewha Womans University, Seoul 120-750, Korea

ABSTRACT: A new class of redox active free base and metalloporphyrins fused with the 1,3-dithiol-2-ylidene subunits present in tetrathiafulvalene, termed **MTTFP** (M = H_2, Cu, Ni, Zn), have been prepared and characterized. The strong electron donating properties of **MTTFP** were probed by electrochemical measurement and demonstrated the oxidation potentials can be tuned by metalation of the free base form, **H_2TTFP**. X-ray crystal structures of **H_2TTFP, ZnTTFP, CuTTFP,** and the two-electron oxidized species (**CuTTFP^{2+}**) revealed that a severe saddle shape distortion was observed with the dithiole rings bent out of the plane towards one another in the neutral form. In contrast, the structure of **CuTTFP^{2+}** is planar, corresponding to a change from a nonaromatic to aromatic structure upon oxidation. A relatively large two-photon absorption (TPA) cross-section value of **H_2TTFP^{2+}** (1200 GM) was obtained for the free base compound, a value that is much higher than those typically seen for porphyrins (<100 GM). Augmented TPA values for the metal complexes were also seen. The strong electron donating ability of **ZnTTFP** was further enhanced by binding of Cl^- and Br^- as revealed by thermal electron-transfer between **ZnTTFP** and Li^+–encapsulated C_{60} ($Li^+@C_{60}$) in benzonitrile, which was "switched on" by the addition of either Cl^- or Br^- (as the tetrabutylammonium salts). The X-ray crystal structure of Cl^--bound **ZnTTFP** was determined and provided support for the strong binding between the Cl^- anion and the Zn^{2+} cation present in **ZnTTFP**.

Introduction

Precise control and thorough understanding of the electronic structure and reactivity of redox active molecules is of significant importance for the development of new catalysts and charge-separation devices, among other applications.[1-4] The exceptional optoelectronic and redox properties of porphyrins have driven efforts to prepare derivatives with more than one accessible and well-defined electronic state (e.g., aromatic, nonaromatic, and antiaromatic). In recent years, this challenge has been met in a number of instances via the use of so-called expanded porphyrins, analogues of porphyrins containing larger conjugated peripheries or a greater number of pyrrolic subunits than present in porphyrins.[5] However, there remains a need for smaller, electronically switchable materials that more closely resemble porphyrins. Of particular interest would be systems that provide for precise, tunable control of the redox potential over a range that allows for thermal electron transfer interactions with common donors or acceptors. Also of interest would be simple-to-prepare porphyrin analogues that allow access to stable 4n and 4n + 2 π-electron configurations, as well as intermediate 4n +1 radical states.

Recently, we reported that a sterically restricted "rosarin", a hexapyrrolic expanded porphyrin, is capable of transitioning between its antiaromatic and reduced aromatic electronic forms via a stable one-electron oxidized radical state.[6] However, we are unaware of any tetrapyrrolic species that allow access to an analogous 4n + 1 π-electron radical oxidation state and which permit switching between two different closed shell electronic states under standard laboratory conditions. Such putative tetrapyrrolic species are attractive since, in principle, their redox properties could be tuned by metalation as observed for normal porphyrins. Further fine-tuning of the redox properties could likewise be achieved by coordination of an axial ligand to a bound metal center.[7]

Here we report a new π-extended analogue of tetrathiafulvalene[8] (TTF), namely the bis(1,3-dithiol-2-ylidene) quinoidal porphyrin (**H_2TTFP**) and its Cu(II), Ni(II), and Zn(II) derivatives (**MTTFP**; M = Cu^{II}, Ni^{II}, and Zn^{II}). In previous work, we reported TTF-bearing porphyrins wherein the TTF subunits were directly annulated to the porphyrin core.[9] **MTTFP** differs from these earlier systems in that it is a direct "extended" analogue of TTF. As such, it was expected to combine the desirable optical features of the known, but not extensively studied, quinoidal porphyrins[10] with the redox

features of the so-called "exTTF" class of compounds (e.g., 9,10-bis(1,3-dithiol-2-ylidene)-9,10-dihydro-anthracene).[11] As detailed below, this combination permits access to three stable oxidation states, as well as to the rich metalation chemistry of porphyrins. This latter attribute allows the electronic and redox properties of **MTTFP** to be tuned without additional synthetic modification. Additionally, complexation of either a chloride or bromide anion to a bound metal center permits fine-tuning of the redox properties of the **MTTFP**. This, in turn, enables control of electron transfer reactions, including specifically thermal processes involving transfer of an electron from **ZnTTFP** to Li^+–encapsulated C_{60} ($Li^+@C_{60}$) in benzonitrile (PhCN). This combination of chemical features, as well as the separate metal- and anion-based control of the redox properties is not possible with the previously reported ex-TTF systems. Nor, is it attainable with simple porphyrin derivatives. A further notable feature of the present system is that, in contrast to unmodified and dithiole-free quinoidal porphyrins, the **MTTFPs** reported herein display relatively large two-photon absorption (TPA) cross-section values.

Results and Discussion

Scheme 1. Synthesis of H_2TTFP and its Metal Derivatives, MTTPS

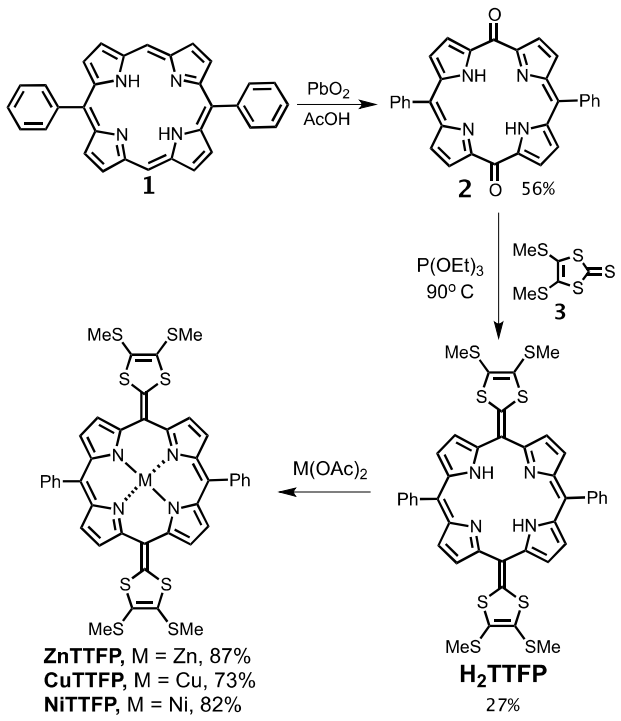

Synthesis of MTTFP. The synthesis of **H_2TTFP** is shown in Scheme 1. It involves as the key step the triethylphosphite-mediated cross-coupling between diketoporphyrinogen **2** and the known TTF precursor **3**.[33] The Lindsey group has previously reported the preparation of **2**, through a thallium promoted oxidation of 5,15-diphenylporphine (**1**).[12] However, in our hands, we found that compound **2** was more conveniently prepared (1 step; 56% yield) by treating **1** with PbO_2 in accord with a decades old procedure for the synthesis of xanthoporphryinogen.[13] Coupling of **2** and **3** then afforded the desired product **H_2TTFP**, as an intensely colored dark green solid in 27% yield. The zinc(II) (**ZnTTFP**), copper(II) (**CuTTFP**), and nickel(II) (**NiTTFP**) complexes were then obtained in good yields by subjecting the free-base to standard acetate salt metal insertion.[14]

A quinoidal structure, such as the one assigned to diketone **2**, was assigned to **H_2TTFP** and its metalated derivatives after examination of the ^{1}H NMR spectrum. Although *tautomerization* of the exocyclic double bonds would result in a fully conjugated core, **H_2TTFP** appears to be non-aromatic. This is consistent with what has been observed in the case of recently reported alkylidene porphyrins[10] and is specifically supported by the fact that the N-H protons within the porphyrinoid core resonate at 12.5 ppm (Figure 1; note that the full spectrum is shown in Figure S1 in the Supporting Information (SI)). In addition, the outer β-C-Hs of the pyrrolic rings give rise to signals at 6.5 and 6.9 ppm. Consequently, the ^{1}H NMR spectrum is strongly indicative of a lack of diatropic ring current**,** and a corresponding lack of aromaticity in **H_2TTFP**. A non-aromatic quinoidal core is thus taken to be the dominant species in solution.

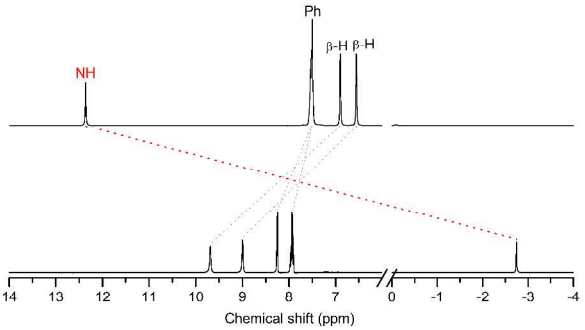

Figure 1. Partial ^{1}H NMR spectra of **H_2TTFP** (top) and **H_2TTFP•2PF$_6$** (bottom) recorded in DMSO-d_6 at 298 K.

Spectroscopic Studies of MTTFP. In the case of **MTTFP** (M = Zn, Cu, Ni), evidence for metal complexation came from high-resolution mass spectrometric (HRMS) analyses. The ^{1}H NMR spectra of the diamagnetic Ni(II) and Zn(II) complexes revealed spectral patterns and chemical shifts similar to those for the corresponding β-pyrrolic and *meso*-phenyl proton signals of **H_2TTFP** (Figures S3–S5). A lack of N-H proton resonances is consistent with metal coordination within the macrocyclic core present in **H_2TTFP.** On the basis of these spectroscopic analyses, the resulting complexes, **ZnTTFP** and **NiTTFP** were also assigned a quinoidal structure analogous to **H_2TTFP**.

An EPR spectrum of **CuTTFP** recorded in CH_2Cl_2 at 298 K is typical of what is expected for a square planar Cu(II) complex with hyperfine interactions between the d^9 configured copper ion and the four magnetically equivalent ^{14}N atoms of the ligand (Figure 2a). The near-perfect agreement between the observed and simulated spectra was obtained with the isotropic g value of g = 2.090 and super-hyperfine splitting of a(Cu) = 91 G, a(N) = 16 G by changing the linewidth (ΔH_{msl}) depending on the m_I values of Cu (Figures 2b and 2c). The observed a(Cu) value is smaller than those of typical Cu(II) porphyrin complexes.[15] This difference is ascribed to the fact that the unpaired electron density in **CuTTFP** is largely centered on the macrocycle and the associated orbital has d_{x2-y2} character. This acts to delocalize ca. 50% of the spin density away from the copper center, as in-

ferred from the theoretical spin density map obtained from UB3LYP/LanL2DZ calculations (Figure 2d).

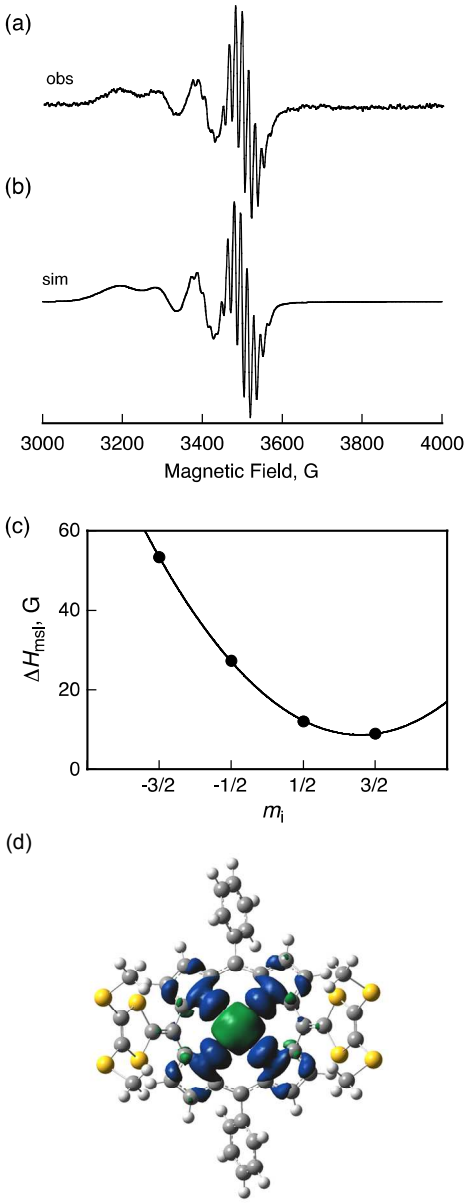

Figure 2. (a) ESR spectrum of **CuTTFP** recorded in CH_2Cl_2 at 298 K, (b) the computer simulated spectrum; a(Cu) = 91 G, a(4N) = 16 G, DH_{msl} = 53, 27, 12, and 9.0 G at m_i = -3/2, -1/2, 1/2 and 3/2, respectively, (c) plot of ΔH_{msl} vs m_i, and (d) spin density map obtained from UB3LYP/LanL2DZ calculations.

The UV-visible spectrum of **H_2TTFP** recorded in CH_2Cl_2 at 298 K supports the assignment of the system as being non-aromatic. For instance, broad absorption bands are seen at λ_{max} = 650 nm (ε = 58000 M^{-1}), 429 nm (ε = 53700 M^{-1}), and 317 nm (ε = 38700 M^{-1}) (Figure 3). These spectral features resemble those of the reported quinoidal porphyrins.[16] The molecular orbitals (MOs), obtained from B3LYP/6-31G(d) calculations, provide support for the conclusion that the highest occupied MO (HOMO) is mainly localized on the dithiole subunits. In contrast, the lowest unoccupied MO (LUMO) is primarily centered within the macrocycle. This is taken as evidence that the observed optical transition includes a contribution involving an intramolecular charge transfer from the dithiole subunits to the central macrocyclic core (cf. Figure S7).[17] Upon metalation, similar low energy broad absorption bands are seen (Figure 3) above 650 nm. The order of the red-shift in these energy transitions is as follows: **ZnTTFP** > **CuTTFP** > **NiTTFP**. In the case of **ZnTTFP**, a small intense band around 850 nm is typically seen in the UV-vis spectrum. This band is thought to reflect the presence of a radical cation impurity formed in small amounts under ambient aerobic conditions. The redox properties and dedicated formation of this and other oxidized forms of MTTFP are discussed later on in the text.

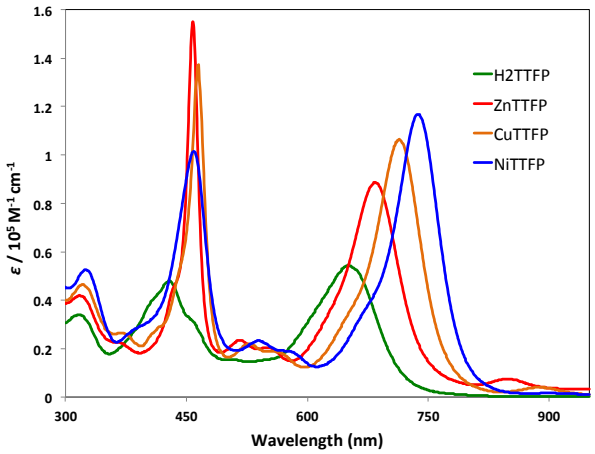

Figure 3. UV/Vis absorption profiles of the metal derivatives of **H_2TTFP** recorded in CH_2Cl_2 including **ZnTTFP** (red), **CuTTFP** (orange), and **NiTTFP** (blue).

The excited state dynamics of **H_2TTFP** were further explored by femtosecond (fs) transient absorption (TA) spectroscopy in toluene. The transient species produced from **H_2TTFP** by fs laser irradiation at 650 nm exhibited both broad excited state absorption (ESA) and ground state bleaching (GSB) features across the entire spectral region as shown in Figure 4a. The temporal profile of the prominent GSB signal at 660 nm was fitted to a biexponential function. This fitting revealed a short time constant of ≈77 ps, as well as a longer time constant (>500 ps) ascribed to a subsequent transition to the triplet manifold. Presumably, this latter intersystem crossing reflects the heavy atom effect of the sulfur atoms.

The TPA spectrum of **H_2TTFP** was also recorded in CH_2Cl_2 using the open aperture z-scan method (Figure 5a and 5b). This analysis revealed spectral features coincident with the lowest one-photon absorption band. The maximum TPA cross-section value, $\sigma^{(2)}$ = 1700 GM, was attained upon excitation at 1400 nm. This value is notably larger than those for analogous (but dithiole-free) quinoidal porphyrins ($\sigma^{(2)}$ = ca. 500 GM at 1200 nm).[16] We propose that the unusual σ-donor-π-acceptor-σ-donor structure of **H_2TTFP** gives rise to the relatively enhanced nonlinear optical response. The TPA properties of the metal complexes, **MTTFPs (M = Zn, Ni, Cu)** were also examined (Figure S9). The **ZnTTFP** ($\sigma^{(2)}$ = 1100 GM at 1300 nm), **NiTTFP** ($\sigma^{(2)}$ = 510 GM at 1300 nm) and **CuTTFP** ($\sigma^{(2)}$ = 450 GM at 1300 nm) complexes gave values that were reduced compared to **H_2TTFP**, but still rela-

tively large with respect to the corresponding metalated porphryins.[18]

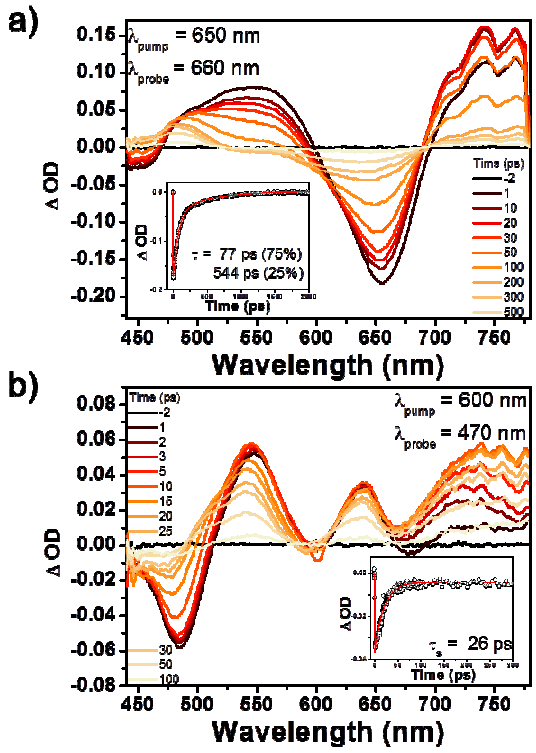

Figure 4. Femtosecond transient absorption spectra and decay profiles of (a) free base **H_2TTFP** recorded in toluene at 298 K and (b) **H_2TTFP•2ClO$_4$** recorded in acetonitrile at 298 K obtained following excitation at 650 and 600 nm, respectively.

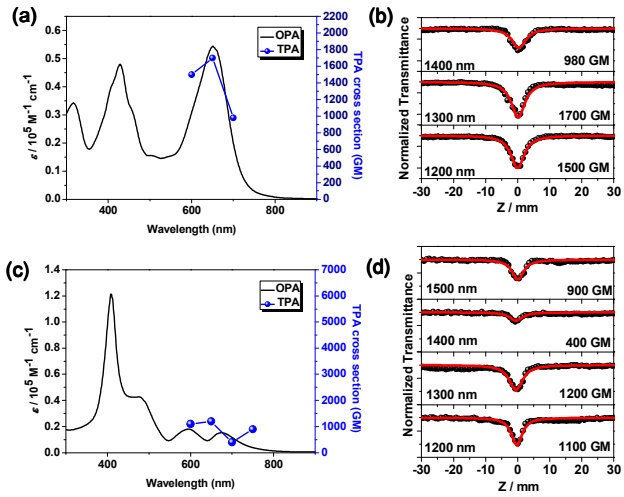

Figure 5. One-photon absorption (OPA) and two-photon absorption (TPA) spectra of (a) **H_2TTFP** and (c) **H_2TTFP•2ClO$_4$** with (b and d) Z-scan curves recorded in CH_2Cl_2 and acetonitrile, respectively at 298 K.

Crystal Structures and Redox Properties of MTTFP. Single crystals suitable for X-ray diffraction analysis of **H_2TTFP** (1:1 mixture of CH_2Cl_2 and acetonitrile), **CuTTFP** (CH_2Cl_2), and **ZnTTFP** (1:1 mixture of CH_2Cl_2 and tetrahydrofuran) were grown by slow evaporation. In all cases, a severe saddle shape distortion was seen with the dithiole rings bent out of the plane towards one another (cf. Figures 6a-b and Figure S10). A distinct lack of planarity is evident. Such a finding provides support for the conclusion drawn from the spectroscopic analyses, namely that the **MTTFP**s are non-aromatic.

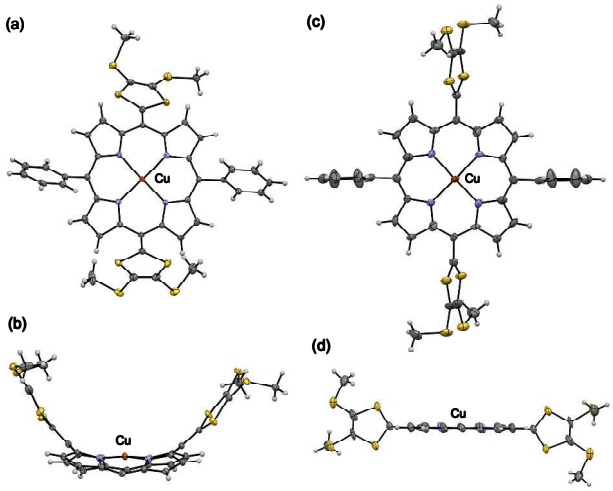

Figure 6. Crystal structures of **CuTTFP** (a) front view and (b) side views and of **CuTTFP•2OTf** (c) front view and (d) side views. The thermal ellipsoids represent 50% probability. The triflate counteranions of **CuTTFP•2OTf** and *meso*-phenyl groups (in the side views) are omitted for clarity.

The electrochemical properties of **H_2TTFP** and its metalated counterparts were further analyzed by cyclic voltammetry (CV) (Figure 7). In the case of the free base, **H_2TTFP**, a redox wave at -0.01 V (vs Fc/Fc^+) was seen. A cathodic/anodic peak separation of 215 mV was also seen in the case of the metal-free system. This was taken as initial evidence that a large conformational change occurs during this redox process. Shifts in the oxidation potentials were seen upon metalation. The nickel complex, **NiTTFP** displayed a nominal shift of -0.008 V, making it only slightly easier to oxidize than the parent compound, **H_2TTFP**. However, the complexes, **CuTTFP** and **ZnTTFP** displayed marked anodic shifts to -0.186 V and -0.245 V, respectively. These findings provide support for the notion that the oxidation potential of the bis-dithiole quinoidal porphyrin **H_2TTPF** can be tuned by simple metal cation complexation.

Insight into the number of electrons being transferred during the oxidation of **H_2TTFP** and its metalated counterparts was inferred from the full CV of **CuTTFP** recorded in CH_2Cl_2 (Figure 8 and Figure S14). A reversible one-electron feature ascribed to the reduction of **CuTTFP** is observed at -1.580 V whose size is approximately half that of the TTFP oxidation peaks; on this basis we propose that twice as many electrons are being transferred (2 e^-) in the TTFP oxidation than in the Cu reduction (1 e^-).[19]

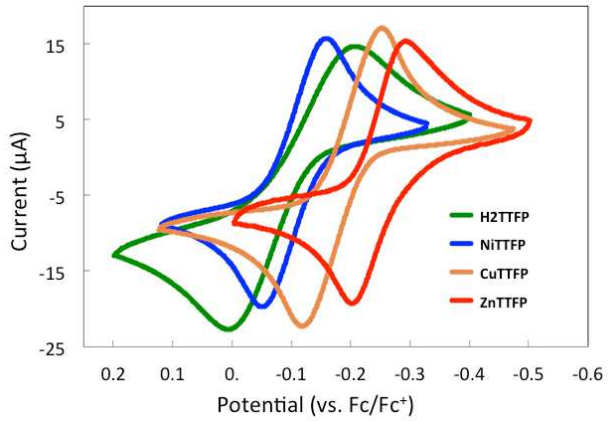

Figure 7. (a) Cyclic voltammograms (CVs) of **H_2TTFP**, **NiTTFP, CuTTFP**, and **ZnTTFP** ($E_{1/2}$ = -0.097, -0.105, -0.186 and -0.245 vs ferrocene/ferrocenium couple (Fc/Fc^+), respectively). All CVs were recorded in CH_2Cl_2 at 298 K under identical conditions: 50 mV/s scan rate, 1 mM solution of the compound under study, 100 mM $TBAPF_6$.

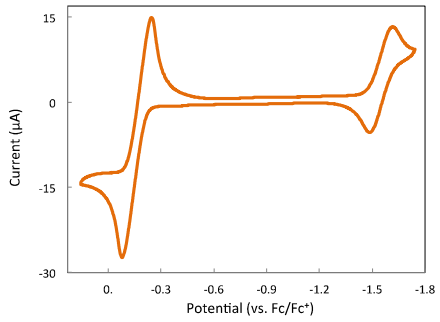

Figure 8. Cyclic voltammogram (CV) showing the first oxidation and reduction features of **CuTTFP** (referenced to Fc/Fc^+). The CV was recorded in CH_2Cl_2 at 298 K: 50 mV/s scan rate, 1 mM solution of the compound under study, 100 mM $TBAPF_6$.

Chemical Oxidation of H_2TTFP. The doubly oxidized form of **H_2TTFP** could also be prepared by chemical means (Scheme 2). Specifically, it was found that by dissolving **H_2TTFP** in CH_2Cl_2 and adding an excess of crystalline nitrosyl hexafluorophosphate, the oxidized product could be precipitated from solution in quantitative yield in the form of its PF_6 salt (**H_2TTFP•2PF$_6$**). In a similar fashion, complexes with other counteranions were easily obtained by altering the identity of the oxidant used. The conversion of **H_2TTFP** to **H_2TTFP^{2+}** gave rise to distinctive spectral changes. In the ^{1}H NMR spectrum (Figure 1) of the dication, **H_2TTFP•2PF$_6$**, the N-H protons are shifted upfield to –2.8 ppm, while the *β*-hydrogens on the porphyrin core are shifted downfield. These changes are thought to reflect the macrocyclic diamagnetic ring current of the central tetrapyrrolic unit. The negative NICS(0) values of −12.1 ppm at the center of the core macrocycle of **H_2TTPF^{2+}** provides further support for the assignment of **H_2TTFP^{2+}** as being aromatic (cf. Figure S13).

A single crystal X-ray diffraction structure of the doubly oxidized dication species derived from **CuTTFP** (i.e., **CuTTFP•2OTf**) revealed a highly planar geometry (Figures 6c-d and S15). The bond lengths between the dithiole rings and the *meso*-carbon atom of porphyrin also increased upon oxidation, as would be expected for the conversion of a $C(sp^2)$=$C(sp^2)$ double bond (average length = 1.364 Å in the case of **CuTTFP**) to a single bond (length = 1.48 Å from **CuTTFP•2OTf**). These structural features are thus consistent with the proposed aromatic formulation.

The steady-state UV-vis absorption spectrum of **H_2TTFP•2PF$_6$**, recorded in acetonitrile at 298 K, revealed features characteristic of a porphyrin (e.g., tetraphenylporphyrin). For instance, well resolved Q-like bands and an intense Soret band at 410 nm (ε = 121000 M^{-1}) were seen (Figure 5b). The porphyrin-like MO density distributions of **H_2TTFP^{2+}** is in good agreement with the experimental spectrum (Figure S16 and S17).[20] However, differences from normal porphyrins were revealed in the fs TA spectra of the dication as recorded in acetonitrile. In particular, an ultrashort singlet excited state lifetime of 26 ps (with a component with a prolonged decay profile ascribed to population of the triplet state) was seen in Figure 4b. This short lifetime[21] is consistent with the non-fluorescent nature of the dication and is thought to reflect electronic coupling with the dithiole moieties.

Further underscoring the differences relative to porphyrins (taken as ostensibly analogous control aromatic systems) is the relatively large TPA cross-section value of **H_2TTFP^{2+}**. Specifically, a TPA value of 1200 GM was recorded upon excitation at 1300 nm (Figures 5c and 5d). These values are considerably higher than those typically seen for porphyrins for which TPA values of <100 GM are found.[18] These differences are ascribed to the charged dithiole sites that serve to perturb the intrinsic electronic structure of the central porphyrin core present in **H_2TTFP^{2+}**.[22]

Scheme 2. Stepwise oxidation of H_2TTFP.

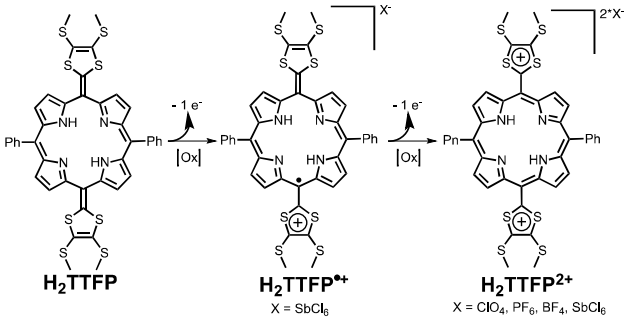

The singly oxidized radical cation form, **$H_2TTFP^{\bullet+}$**, could be prepared *in situ* by the careful addition of tris(4-bromophenyl)aminium hexachloroantimonate (so-called "magic blue") in CH_2Cl_2.[23] The formation of a species with an intense absorption band at 930 nm was seen, with a maximal intensity being observed upon the addition of one equiv of oxidant (Figure 9).[24] When less than one molar equivalent of magic blue is added, a species with an absorption maximum (λ_{max}) at 760 nm is observed. This peak is thought to reflect protonation of **H_2TTFP** (for which enhanced acidity is expected due to the saddle-type distortion of the porphyrinoid core[24]) by residual acid present in the oxidant.[25] Support for this suggestion comes from the observation that adding trifluoroacetic acid to the free-base species **H_2TTFP** in the

absence of magic blue likewise gives rise to an analogous 760 nm spectral feature while leading to a decrease of the original absorption peak at 650 nm (Figure S18). Furthermore, chemical oxidation of **ZnTTFP** (which lacks the basic pyrrolic sites present in **H_2TTFP)** with magic blue fails to produce a species with a $\lambda_{max} \approx 760$ nm (Figure S19).

Electron paramagnetic resonance (EPR) spectroscopic analysis of **H_2TTFP$^{\bullet+}$** (930 nm absorption band) revealed features at $g_{\perp} = 2.001$ and $g_{//} = 2.006$ at 77 K,[26] thus supporting assignment of this oxidized species to the radical cation. Such readily accessible 4n + 1 π-electron radical cation species are not attainable with either simple quinoidal porphyrins or the anthracene-derived exTTF species reported earlier. The behavior of **MTTFP** also stands in contrast to what is seen for the previously reported TTF porphyrins, where TTF-centered, but not porphyrinoid 4n+1 π-electron, radicals may be observed[9]

The stability of **H_2TTFP$^{\bullet+}$** proved to be highly dependent on the choice of solvent. In contrast to what was seen in pure CH_2Cl_2, in polar solvents, such as acetonitrile, PhCN or mixtures of these solvents in CH_2Cl_2, the spectral features corresponding to **H_2TTFP$^{\bullet+}$** were not observed (Figure S20). This is ascribed to disproportionation of the radical cation **H_2TTFP$^{\bullet+}$**. Disproportionation leads to formation of the closed shell neutral and dication forms of **H_2TTFP**, respectively, in analogy to what was found in the exTTFs.[27] An alternative explanation, involving dimerization to form a closed shell, EPR silent dimer (e.g., **[(H_2TTFP)$_2$]$^{2+}$**), is ruled out on steric grounds; the large *meso*-phenyl groups are expected to preclude the necessary intermolecular contact.

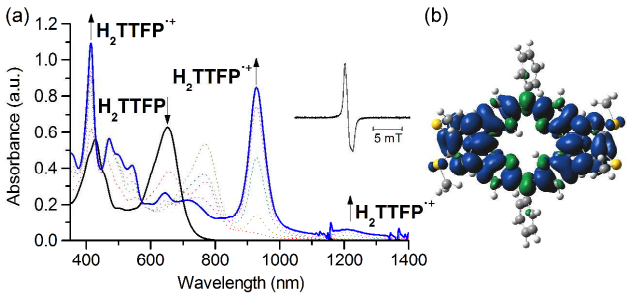

Figure 9. (a) UV/vis/NIR absorption spectra of **H_2TTFP** recorded in CH_2Cl_2 at 298 K in the presence of increasing quantities of magic blue up to one molar equivalent; [**H_2TTFP**] = 10 μM. Inset shows the EPR spectrum of **H_2TTFP$^{\bullet+}$** (as the $SbCl_6^-$ salt) prepared via the addition of 1 equiv of magic blue. (b) Spin density map of **H_2TTFP$^{\bullet+}$** obtained at the UB3LYP/6-31G(d) level.

Fine Redox Control of ZnTTFP by Anion Binding. The strong electron donor ability of **ZnTTFP** is further enhanced by axial coordination of chloride anion, Cl^- as shown via its use as an external donor in a thermal electron transfer reaction. In these experiments, Li^+–encapsulated C_{60} ($Li^+@C_{60}$) was chosen as the electron acceptor, because $Li^+@C_{60}$ has a one-electron reduction potential (i.e., 0.13 V (vs SCE)), which is slightly less positive than that of **ZnTTFP** (cf. Figure 7).[28] No evidence of electron transfer from **ZnTTFP** to $Li^+@C_{60}$ was seen in PhCN at 298 K. Specifically, addition of tetra-*n*-butylammonium perchlorate ($TBAClO_4$: 1.0 mM) to a PhCN solution of **ZnTTFP** and $Li^+@C_{60}$ resulted in no change in the optical features (Figure S21). However, addition of chloride anion as TBACl to a PhCN solution containing **ZnTTFP** and $Li^+@C_{60}$ resulted in thermal electron transfer from **ZnTTFP** to $Li^+@C_{60}$. This is evidenced by the generation of spectral features ascribable to **ZnTTFP$^{\bullet+}$** (λ_{max} = 865 nm) and $Li^+@C_{60}^{\bullet-}$ (λ_{max} = 1035 nm) as seen in Figure 10a.[28] The 1:1 stoichiometry of electron transfer between **ZnTTFP** and $Li^+@C_{60}$ in the presence of TBACl was confirmed by a Job plot (Figure S22). The formation of **ZnTTFP$^{\bullet+}$** and $Li^+@C_{60}^{\bullet-}$ was further confirmed by EPR spectral analyses, which revealed a superposition of signals corresponding to both species (Figure S23). The yield of the electron-transfer products increased with increasing concentration of $Li^+@C_{60}$. The electron-transfer equilibrium constant (K_{et}), determined from the titration shown in Figure 10b, is 0.53.

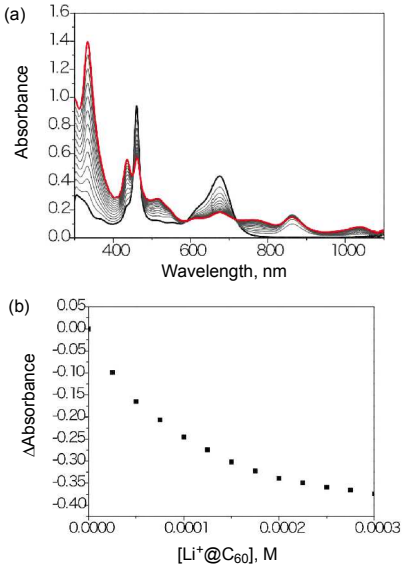

Figure 10. (a) UV/vis absorption changes in electron transfer from **ZnTTFP** (10 μM, black) to $Li^+@C_{60}$ (final: red) in the presence of 1.0 mM TBACl in PhCN at 298 K. (b) Plot of absorbance at 460 nm vs the concentration of $Li^+@C_{60}$.

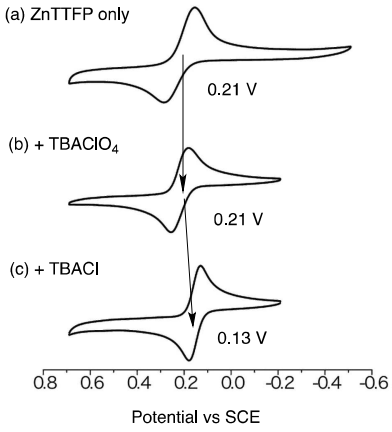

Figure 11. (a) Cyclic voltammogram (CV) of **ZnTTFP** (0.10 mM) recorded in the presence of $TBAPF_6$ (100 mM) in PhCN. (b) CV of **ZnTTFP** in the same solvent after the addition of $TBAClO_4$ (20 mM). (c) CV of ZnTTFP recorded under identical conditions after addition of TBACl (20 mM).

The negative shift in the (two-electron) oxidation potential (E_{ox}) of **ZnTTFP** induced by binding of Cl^- was confirmed

by **CV** measurements, as shown in Figure 11. The E_{ox} value of **ZnTTFP** in the presence of $TBAPF_6$ in PhCN was determined to be 0.21 V vs SCE. The E_{ox} value remained the same after the addition of $TBAClO_4$. However, the addition of TBACl resulted in a cathodic shift of the E_{ox} value to 0.13 V vs SCE. Since the E_{red} value of $Li^+@C_{60}$ is 0.13 V vs SCE, electron transfer from **ZnTTFP** to $Li^+@C_{60}$ becomes thermodynamically feasible as the result of the complexation of the Cl^- anion to **ZnTTFP**. The binding of Cl^- to **ZnTTFP** was confirmed via a single crystal X-ray diffraction analysis. The resulting structure, shown in Figure 12, reveals that the Cl^- is coordinated to the Zn^{2+} center present in **ZnTTFP**.

The charge separated species induced by the presence of chloride can be reverted to the neutral form via the addition of excess pyridine; presumably this reflects competitive binding to the zinc center and displacement of the Cl^- ligand (Figure S24). In this "molecular switch", the thermal electron transfer from **ZnTTFP** to $Li^+@C_{60}$ is "turned on" via the addition of chloride and is "turned off" upon treatment with excess pyridine. This provides an additional level of control over a process that is not reflected in the chemistry of either exTTFs or quinoidal porphyrins.

$$\mathbf{ZnTTFP} + Li^+@C_{60} \underset{\text{Pyridine}}{\overset{Cl^-}{\rightleftharpoons}} [\mathbf{Zn(Cl)TTFP}]^{+\bullet} + [Li@C_{60}]^{\bullet}$$

As would be expected, complexation of Br^- to **ZnTTFP** also appears to be facile. This is evidenced by the fact that the addition of TBABr to a premixed PhCN solution of **ZnTTFP** and Li+@C_{60} also results in electron transfer from **ZnTTFP** to $Li^+@C_{60}$ in analogy to what is seen for Cl^- (Figure S25).

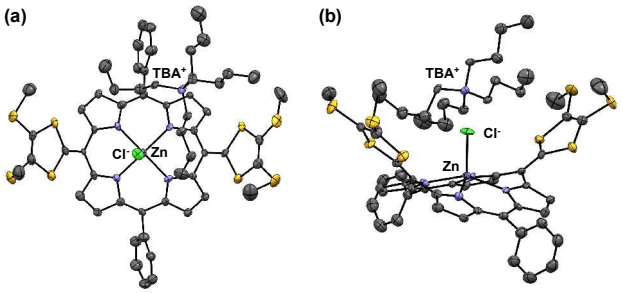

Figure 12. Two views of the single crystal X-ray diffraction structure of **ZnTTFP•TBACl** at 50% thermal ellipsoids probability level. The solvent of crystallization and the hydrogen atoms are omitted for clarity.

Conclusion

In conclusion, we have synthesized a new class of quinoidal porphyrin analogues (**MTTFP**) capable of existing in three distinct oxidation states each separated by one-electron. When subject to two-electron oxidation, aromatization is induced. This leads to conversion from a saddle-shaped nonaromatic species to a planar aromatic dicationic porphyrin, which exhibits a relatively large TPA cross-section value. The redox potentials of **MTTFP** may be tuned by metalation, with the associated electrochemical analyses revealing that **MTTFP** should be capable of acting as a strong electron donor. A particular advantage of these systems is that they are readily metalated and as demonstrated by the zinc complex **ZnTTFP** can ligate an axial ligand, thereby allowing the electronic properties to be tuned via two different modes (metal complexation and anion coordination). In the case where Cl^- or Br^- was bound to the zinc center of **ZnTTFP**, the electron donor ability of the complex was further enhanced and this fine-tuning makes possible electron transfer from **ZnTTFP** to $Li^+@C_{60}$. Upon addition of pyridine to the chloride complex, back electron transfer took place, demonstrating the necessity of the Zn-halide bond for the forward reaction, as well as the versatility of the system.

The salient features of the **MTTFP**s, namely access to three distinct 4n + y (y = 0, 1, 2) π-electron configurations, fine-tuning of the redox features through metal coordination and anion complexation, thermal electron transfer to $Li^+@C_{60}$, and high TPA values, are not observed in the case of either other easy-to-access tetrapyrrolic derivatives (including quinoidal porphyrins and TTF-porphyrins) or the anthracene-derived exTTF systems. We thus think that present systems may have a role to play in advancing our understanding of how modifications of relatively simple structures can be translated into potentially useful properties and electronic applications.

Experimental Section

Materials and General Methods. All chemicals were obtained from Acros chemicals or TCI America in reagent grade purity and used without further purification unless otherwise noted. PhCN was distilled over P_2O_5 immediately before use, collecting the middle 50%. Proton (400 MHz) and ^{13}Carbon (100 MHz) NMR spectra were measured using a Varian 400/54/ASW instrument. Chemical shifts (δ-scale) are reported in ppm relative to residual solvent and internal standard signals (DMSO-d_6: 2.50 ppm and acetone-d_6: 2.05 ppm for ^{1}H, and CD_3Cl: 77.2 ppm, and CD_3CN: 1.3 ppm for ^{13}C). UV-Vis-NIR spectra were recorded on a Cary 5000 spectrometer in a 1 cm quartz cuvette. HRMS were recorded on an Agilent 6530 Accurate Mass QTOF/LC-MS (ESI) and a Ionospec 9.4 FT-ICR (MALDI).

Electrochemical Measurements. All electrochemical measurements were carried out using a CV-50 electrochemical analyzer in dichloromethane (CH_2Cl_2) at 298 K using 0.1 M $TBAPF_6$ as the supporting electrolyte. A glassy carbon working electrode was used, as well as a platinum wire counter electrode and an Ag/AgCl or $Ag/AgNO_3$ reference electrode. The working electrode was routinely polished using standard polishing procedures.

EPR Measurements. The EPR spectra were recorded on a JEOL X-band spectrometer (JES-RE1XE) under non-saturating microwave power conditions (1.0 mW) operating at 9.2 GHz. The magnitude of the modulation was chosen to optimize the resolution and the signal to noise ratio (S/N) of the observed spectrum (modulation width, 20 G; modulation frequency, 100 kHz). The *g* values were calibrated using an Mn^{2+} marker.

Femtosecond Transient Absorption Measurements. The femtosecond time-resolved transient absorption (TA) spectrometer consisted of NIR optical parametric amplifier (OPA) system (Quantronix, Pallitra) pumped by a Ti:sapphire regenerative amplifier system (Quantronix, Integra-C) operating at 1 kHz repetition rate and an optical detection system. The generated OPA output signals had a pulse width of ~ 100

fs in the range of 480-700 nm which were used as pump pulses. White light continuum (WLC) probe pulses were generated using a sapphire window (3 mm of thickness) by focusing of small portion of the fundamental 800 nm pulses. The time delay between pump and probe beams was carefully controlled by making the pump beam travel along a variable optical delay (Newport, ILS250). Intensities of the spectrally dispersed WLC probe pulses are monitored by two miniature spectrographs (OceanOptics USB2000+). To obtain the time-resolved transient absorption difference signal (ΔA) at a specific time, the pump pulses were chopped at 25 Hz and absorption spectra intensities were saved alternately with or without the pump pulse. Typically, 6000 pulses were used to excite the samples to obtain the TA spectra at a particular delay time. The polarization angle between pump and probe beam was set at the magic angle (54.7°) in order to prevent polarization-dependent signals. Cross-correlation fwhm in pump-probe experiments was less than 200 fs and chirp of WLC probe pulses was measured to be 800 fs in the 400-1200 nm region. To minimize chirp, all reflection optics were used in the probe beam path and a 2 mm path length quartz cell was employed. After the TA experiments, the absorption spectra of all compounds were carefully checked so as to avoid artifacts arising from, e.g., photo-degradation or photo-oxidation of the samples in question.

Two-Photon Absorption Experiments. Two-photon absorption (TPA) spectra were measured in the NIR region using the open-aperture Z-scan method with 130 fs pulses from an optical parametric amplifier (Light Conversion, TOPAS) operating at a repetition rate of 2 kHz generated from a Ti:sapphire regenerative amplifier system (Spectra-Physics, Hurricane-X). The NIR beam was divided into two parts. One was monitored by a Ge-PIN photodiode (New Focus) as an intensity reference, and the other was used for the transmittance measurement. After passing through a 10 cm focal length lens, the laser beam was focused and passed through a 1 mm quartz cell. Since the position of the sample cell could be controlled along the laser beam direction (z axis) using the motor-controlled delay stage, the local power density within the sample cell could be simply controlled under constant laser intensity. The transmitted laser beam from the sample cell was then detected by the same photodiode as used for reference monitoring. The on-axis peak intensity of the incident pulses at the focal point, I0, ranged from 40 to 60 GW cm-2. For a Gaussian beam profile, the nonlinear absorption coefficient can be obtained by curve fitting of the observed open-aperture traces T(z) with the following equation:

$$T(z) = 1 - \frac{\beta I_0 (1 - e^{-\alpha_0 l})}{2\sqrt{2}\alpha_0 [1 + (z/z_0)^2]}$$

where α 0 is the linear absorption coefficient, l the sample length, and z0 the diffraction length of the incident beam. After the nonlinear absorption coefficient has been obtained, the TPA cross section σ (2) of one solute molecule (in units of GM, where 1 GM = 10-50 cm4 s photon-1 molecule-1) can be determined by using the following relationship:

$$\beta = \frac{10^{-3} \sigma^{(2)} N_A d}{h\nu}$$

where N_A is the Avogadro constant, d is the concentration of the compound in solution, h is the Planck constant, and ν is the frequency of the incident laser beam.

Density Functional Theory (DFT) Calculations. Theoretical calculations were performed with the Gaussian09 program suite using a supercomputer (KISTI, IBM).[29] All optimized structures were obtained using the density functional theory (DFT) calculations with Becke's three-parameter hybrid exchange functionals and the Lee-Yang-Parr correlation functional (B3LYP) employing the 6-31G(d) basis set for all atoms.[30] The global ring centers for the NICS(0) values were designated at the non-weighted mean centers of the macrocycles. The NICS(0) value was obtained with gauge independent atomic orbital (GIAO) method based on the optimized geometries. To simulate the ground-state absorption spectra, the time-dependent (TD) DFT calculation was employed with (U)B3LYP/6-31G(d) level. In the specific case of dication, 12+, the Handy and co-workers' of long-range corrected TD-CAMB3LYP/6-31G(d) level calculations[31] that gives rise to the consistent transitions for charged derivatives were carried out.

Synthetic Procedures

5,15-Dioxo-10,20-diphenylporphodimethene (2):

5,15-Diphenylporphyrin (**1**) (0.77 g, 1.66 mmol) was dissolved in a mixture of chloroform (100 mL) and acetic acid (20 Ml). A solution of PbO_2 (4.0 g, 16.7 mmol) was added and the reaction mixture was stirred for 5 h open to air, whereafter the mixture was slowly poured into a saturated aqueous sodium bicarbonate solution (300 mL) to quench the acetic acid and the organic and aqueous phase were separated. The organic phase was passed through a short plug of celite to remove residual lead salts. The aqueous layer was extracted twice with dichloromethane (2 x 100 mL) and the two organic fractions were also passed through the celite. The celite was washed thoroughly with dichloromethane until the filtrate was colorless. The combined organic filtrates were evaporated and the residue purified by column chromatography over silica gel using 30% hexanes/dichloromethane as the eluent. The dark yellow band was collected affording .46g (56% yield) of **2** as a black solid. The black crystalline solid could be further purified by recrystallizing from hot toluene. The ^{1}H NMR spectral data matched that reported previously:[30] ($CDCl_3$, 298 K) δ 6.2-2.6 (br s, 4H, β-H), 7.17 (d, J = 4.4Hz, 4H, β-H), 7.35-7.45 (m, 10H, Ph-H), 13.85 (br s, 2H, N-H) ppm.

ExTTF-Porphyrin (H$_2$TTFP):

To a mixture of 5,15-dioxo-10,20-diphenylporphodimethene (**2**) 100 mg, 0.203 mmol) and 4,5-bis(methylthio)-1,3-dithiole-2-thione (**3**)[33] (100 mg, 0.444 mmol) in a dried 100 mL round bottom flask was added freshly distilled triethylphosphite (3 ml) and the reaction mixture was heated slowly to 90 °C under a nitrogen atmosphere. After stirring the reaction mixture for 1 h at 90 °C, another 100 mg (0.444 mmol) aliquot of **3** was added to the reaction mixture. The mixture was stirred for additional 1 h affording a dark green solution. After cooling to room temperature, the reaction mixture was filtrated using a fine fritted glass filter to give a dark green solid as a "first crop". The remaining filtrate was poured into cold methanol (100 mL) and the resulting precipitate was collected by filtration to yield a "second crop". The first crop obtained in this way proved sufficiently pure to be used in further reactions. The second crop was purified by column chromatography over silica gel (to remove the product of the homocoupling of **3**) using 30% hexanes/dichloromethane as the eluent; this provided analytically pure **H$_2$TTFP** (total yield, 102 mg, 27%).

R_f = 0.3. ^{1}H NMR: (acetone-d_6, 298 K) δ 2.48 (s, 12H, S-CH_3), 6.61 (d, J = 4.3 Hz, 4H, β-H), 6.90 (d, J = 4.3 Hz, 4H, β-H), 7.55 (m, 10H Ph-H) 12.59 (s, 2H, NH); ^{13}C NMR ($CDCl_3$, 298 K): δ

19.1, 114.1, 117.9, 127.4, 127.9, 128.5, 129.6, 130.9, 138.0, 140.0, 141.7, 152.3. HRMS-Positive-ESI: m/z 849.04578. Calcd.: 849.04654. MP > 300 °C.

Oxidation of H_2TTFP to H_2TTFP•2PF_6

Freebase **H_2TTFP** (20 mg, 0.024 mmol) was dissolved in a minimal amount of dichloromethane (2 mL). Crystalline $NOPF_6$ (≈ 45 mg, 0.257 mmol) was quickly weighed and added in excess and the reaction was stirred for 15 min. A precipitate was immediately noticeable. After 15 min, the residual solvent proved to be nearly colorless, and at this time the solvent and precipitate were decanted from the leftover solid $NOPF_6$. The solution was filtered and the solids washed with water and dichloromethane until the filtrate was colorless. The solid material was dried under vacuum at RT to give pure **H_2TTFP^{2+}•2PF_6**. ^{1}H NMR (DMSO-d_6, 298 K): δ -2.75 (s, 2H, NH), 3.11 (s, 12H, S-CH_3), 7.92 (m, 6H, Ph-H), 8.24 (dd, J = 1.45, 7.75), 8.99 (br s, 4H, β-H), 9.68 (br s, 4H, β-H). ^{13}C NMR ($CDCl_3$, 125 MHz, 298 K): δ 19.4, 125.9, 127.0, 128.4, 131.3, 134.3, 134.5, 141.4, 148.9, 152.0, 155.5 HRMS-Positive-ESI: z = 1, m/z 849.04693, calcd.: 849.04654. z =2, m/z 425.02727. Calcd.: 425.02691 MP > 300 °C.

General Metalation Procedure for H_2TTFP

Compound **H_2TTFP** (20 mg, 0.024 mmol) was dissolved in dichloromethane (50 ml) and excess metal acetate, $M(OAc)_2$ (100 mg) dissolved in MeOH (1 mL) was added. The solution was stirred for 1 h or until all of **H_2TTFP** was consumed, as judged by TLC analysis. After removal of the solvent, the residue was purified by column chromatography over silica gel to give the target complexes,:

ZnTTFP. Eluent dichloromethane; R_f = 0.8, (87% yield) ^{1}H NMR (DMSO-d_6, 400 MHz, 298 K): δ 2.43 (s, 12H, S-CH_3), 6.40 (d, J = 4.2 Hz, 4H, β-H), 6.85 (d, J = 4.2 Hz, 4H, β-H), 7.47 (m, Ph-H). ^{13}C NMR ($CDCl_3$, 125 MHz, 298 K): δ 19.0 116.3, 117.8, 127.1, 127.5, 128.0, 130.7, 131.6, 139.5, 141.7, 155.7. HRMS-Positive-MALDI: m/z 909.9524, Calcd.: 909.9522. This compound was further analyzed by a single crystal X-ray diffraction analysis. MP > 300 °C.

CuTTFP. Eluent 30% hexanes/dichloromethane; R_f = 0.9, (73% yield). As noted in the main text, the EPR spectrum of this complex is consistent with the proposed structure. A clean HPLC chromatogram of this paramagnetic species was also obtained. HRMS-Positive-MALDI: m/z 908.9516. Calcd.: 908.9527. This compound was further analyzed by a single crystal X-ray diffraction analysis. MP > 300 °C.

NiTTFP. Eluent dichloromethane; R_f = 0.9, (82% yield). ^{1}H NMR (DMSO-d_6, 400 MHz 298K): δ 2.46 (s, 12H, S-CH_3), 6.65 (d, J = 4.5 Hz, 4H, β-H), 6.89 (d, J = 4.5 Hz, 4H, β-H), 7.52 (m, 10H, Ph-H). ^{13}C NMR could not be taken due to precipitation from DMSO-d_6 upon standing over several hours. HRMS-Positive-MALDI: m/z 903.9587. Calcd.: 903.9584. MP > 300 °C.

Preparation of ZnTTFP•TBACl

For absorption and CV studies, **ZnTTFP•**TBACl was prepared *in situ* by the addition of 1.2 molar equivalents of tetrabutylammonium chloride to **ZnTTFP** in PhCN. **ZnTTFP•**TBACl can be isolated as its crystalline salt by the addition of 3 molar equivalents of tetrabutylammonium chloride to **ZnTTFP** in dichlormethane followed by slow diffusion of hexanes at 277 K for several days.

X-ray Crystallography Methods

All data were collected on a Rigaku ACF-12 with a Saturn 724+ CCD and a Rigaku SCX-Mini diffractometer with a Mercury 2 CCD using a graphite monochromator with MoKa radiation (λ = 0.71075 Å). The data were collected at 100 K using a Rigaku XStream low temperature device. Details of crystal data, data collection and structure refinement for each analyzed sample are listed in Table S1-S25 in SI. D\In all cases, the data reduction were performed using the Rigaku Americas Corporation's Crystal Clear version 1.40.[34] Each structure was solved by direct methods using SIR97[35] and refined by full-matrix least-squares on F^2 with anisotropic displacement parameters for the non-H atoms using SHELXL-97.[36] The contributions to the scattering factors due to the solvent molecules were removed by use of the utility SQUEEZE[37] in PLATON98.[38] Structure analysis was aided by use of the programs PLATON98 as incorporated into WinGX.[39] The hydrogen atoms on carbon were calculated in ideal positions with isotropic displacement parameters set to 1.2xUeq of the attached atom (1.5xUeq for methyl hydrogen atoms). Definitions used for calculating R(F), $R_w(F^2)$ and the goodness of fit, S, are given in SI.[40] The data were checked for secondary extinction effects but no correction was necessary. Neutral atom scattering factors and values used to calculate the linear absorption coefficient are from the International Tables for X-ray Crystallography (1992).[41] All figures were generated using SHELXTL/PC.[42] Details of the structures and their refinement may be obtained from the Cambridge Crystallographic Data Centre by referencing CCDC 931728 for **H_2TTFP**, 931726 for **CuTTFP**, 931727 for **CuTTFP•2OTf** 931725 for **ZnTTFP**, 0001834 for **ZnTTFP**(TBACl).

ASSOCIATED CONTENT

Supporting Information. Characterization data for all new compounds and X-ray crystallographic data tables. This material is available free of charge via the Internet at http://pubs.acs.org.

AUTHOR INFORMATION

Corresponding Authors

sessler@cm.utexas.edu (JLS); dongho@yonsei.ac.kr (DK); fukuzumi@chem.eng.osaka-u.ac.jp (SF)

ACKNOWLEDGMENT

Support is acknowledged from the U.S. National Science Foundation (CHE-1057904 to J.L.S.), the Robert A. Welch Foundation (F-1018 to J.L.S.), JSPS (No. 20108010 to S.F), the World Class University (WCU) program (R32-2012-000-10217-0 to D.K, R31-2008-000-10010-0 to S.F.) of the Ministry of Education, Science and Technology, the Villum Foundation (to J.O.J.), and The Danish Natural Science Reasearch Council (FNU, Project No. 11-106744 to J.O.J.).

REFERENCES

(1) (a) Frischmann, P. D.; Mahata, K.; Würthner, F. *Chem. Soc. Rev*. **2013**, *42*, 1847-1870. (b) Li, L.-L.; Diau, E. W.-G., *Chem. Soc. Rev*. **2013**, *42*, 291-304. (b) Panda, M. K.; Ladomenou, K.; Coutsolelos, A. G. *Coord. Chem. Rev*. **2012**, *256*, 2601-2627. (c) Bottari, G.; Trukhina, O.; Ince, M.; Torres, T. *Coord. Chem. Rev*. **2012**, *256*, 2453-2477. (d) Griffith, M. J.; Sunahara, K.; Wagner, P.; Wagner, K.; Wallace, G. G.; Officer, D. L.; Fu-

rube, A.; Katoh, R.; Mori, S.; Mozer, A. J. *Chem. Commun*. **2012**, *48*, 4145-4162.
(2) (a) Wasielewski, Michael R. *Acc. Chem. Res*. **2009**, *42*, 1910-1921. (b) Wasielewski, M. R. *J. Org. Chem*. **2006**, *71*, 5051-5066.
(3) (a) Malig, J.; Jux, N.; Guldi, D. M. *Acc. Chem. Res*. **2013**, *46*, 53-64. (b) Goerl, Daniel; Zhang, Xin; Wuerthner, Frank, *Angew. Chem., Int. Ed.* **2012**, *51*, 6328-6348.
(4) (a) Fukuzumi, S.; Yamada, Y.; Suenobu, T.; Ohkubo, K.; Kotani, H. *Energy Environ. Sci*. **2011**, *4*, 2754-2766. (b) Fukuzumi, S.; Ohkubo, K. *J. Mater. Chem*. **2012**, *22*, 4575-4587. (c) Fukuzumi, S.; Honda, T.; Kojima, T. *Coord. Chem. Rev*. **2012**, *256*, 2488-2502.
(5) (a) Saito, S.; Osuka, A. *Angew. Chem. Int. Ed*. **2011**, 50, 4342-4373. (b) Osuka, A.; Saito, S. *Chem. Commun.* **2011**, 47, 4330-4339. (c) Roznyatovskiy, V.V.; Lee, C.-H.; Sessler, J. L. *Chem. Soc. Rev*. **2013**, 42, 1921-1933.
(6) Ishida, M.; Kim, S.-J.; Preihs, C.; Ohkubo, K.; Lim, J. M.; Lee, B. S.; Park, J. S.; Lynch, V. M.; Roznyatovskiy, V. V.; Sarma, T.; Panda, P. K.; Lee, C.-H.; Fukuzumi, S.; Kim, D.; Sessler, J. L. *Nat. Chem*. **2013**, *5*, 15-20.
(7) (a) *The Porphyrin Handbook, Vol 3, Inorganic, Organometallic, and Coordination Chemistry;* Kadish, K.M.; Smith, K.M.; Guilard, R. Eds.; Academic Press: San Diego, 2000. (b) Park, J. S.; Karnas, E.; Ohkubo, K.; Chen, P.; Kadish, K. M.; Fukuzumi, S.; Bielawski, C.; Todd W. Hudnall, T. W.; Lynch, Sessler, J. L. *Science* **2010**, *329*, 1324-1327. (c) Fukuzumi, S.; Ohkubo, K.; D'Souza, F.; Sessler, J. L. *Chem. Commun*. **2012**, *48*, 9801-9815.
(8) (a) Schukat, G.; Fanghänel, E. *Sulfur Rep.* **1996**, *18*, 1–294. (b) Bryce, M. R. *J. Mater. Chem.* **2000**, *10*, 589–598. (c) Segura, J. L.; Martín, N. *Angew. Chem. Int. Ed.* **2001**, *40*, 1372–1409. (d) Jeppesen, J. O.; Nielsen, M. B.; Becher, J. *Chem. Rev.* **2004**, *104*, 5115–5132. (e) Inagi, S.; Naka, K.; Chujo, Y. *J. Mater. Chem.* **2007**, *17*, 4122–4135. (f) Martín, N.; Sánchez, L.; Herranz, M. a. Á.; Illescas, B.; Guldi, D. M. *Acc. Chem. Res.* **2007**, *40*, 1015–1024. (g) Lorcy, D.; Bellec, N.; Fourmigué, M.; Avarvari, N. *Coord. Chem. Rev*. **2009**, *253*, 1398–1438.
(9) (a) J. Becher, T. Brimert, J. O. Jeppesen, J. Z. Pedersen, R. Zubarev, T. Bjørnholm, N. Reitzel, T. R. Jensen, K. Kjaer, E. Levillain *Angew. Chem. Int. Ed.* **2001**, *40*, 2497−2500. (b) H. Li, J. O. Jeppesen, E. Levillain, J. Becher *Chem. Commun.* **2003**, 846−847. (c) K. A. Nielsen, E. Levillain, V. M. Lynch, J. L. Sessler, J. O. Jeppesen *Chem. Eur. J.* **2009**, *15*, 506−516. (d) Jana, A.; Ishida, M.; Kwak, K.; Sung, Y.M.; Kim, D.-S.; Lynch, V.M., Lee, D.; Kim, D.; Sessler, J.L. *Chem. Eur. J.* **2013**, 19, 338-349.
(10) Lee, C.-H.; Roznyatovskiy, V. V.; Hong, S.-L.; Sessler, J. L. in *Handbook of Porphyin Science,* Kadish, K.M.; Smith, K. M.; Guilard, R. Eds.; World Scientific, Singapore, 2011, pp 197-252.
(11) (a) *TTF Chemistry*, Yamada, J.; Sugimoto, T. Eds.; Kodansha Ltd.: Tokyo, 2004. (b) Brunetti, F. G.; Lopez, J. L.; Atienza, C.; Martin, N. *J. Mater. Chem.* **2012**, 22, 4188-4205.
(12) Lahaye, D.; Muthukumaran, K.; Hung, C-H.; Gryko, D; Reboucas, J. S.; Spasojevic, I.; Batinic-Haberle, I.; Lindsey, J. S. *Bioorg. Med. Chem.* **2007**, *15*, 7066-6086.
(13) (a) Fischer, H.; Treibs, A. *Annalen* **1927**, *457*, 209-248. (b) Inhoffen, H. H.; Fuhrhop, J. R.; von der Haar, F. *Justus Liebigs Ann. Chem.* **1966**, *700*, 92-105.
(14) *The Porphyrin Handbook, Vol 1, Synthesis and Organic Chemistry;* Kadish, K.M.; Smith, K.M.; Guilard, MR. Eds.; Academic Press: San Diego, 2000.
(15) Cunningham, K. L.; McNett, K. M.; Pierce, R. A.; Davis, K. A.; Harris, H. H.; Falck, D. M.; McMillin, D. R. *Inorg. Chem*. **1997**, *36*, 608-613.
(16) Zeng, W.; Lee, B. S.; Sung, Y. M.; Huang, K.-W.; Li, Y.; Kim, D.; Wu, J. *Chem. Commun*., **2012**, 48, 7684-7686.
(17) Similar conclusions were drawn in the case of simple exTTF derivatives: e.g. Diaz, M. C.; Illescas, B. M.; Martin, N.; Viruela, R.; Viruela, P. M.; Orti, E.; Brede, O.; Zilbermann, I.; Guldi, D. M. *Chem.–Eur. J.* **2004**, 10, 2067-2077.
(18) TPA cross-section values for reference metalated tetraphenylporphyrins (TPP) have been reported as follows: For ZnTPP: (a) Drobizhev, M.; Karotki, A.; Kruk, M.; Rebane, A. *Chem. Phys. Lett.* **2002**, *355*, 175-182; for NiTPP: (b) Yoon, M.-C.; Noh, S.-B.; Tsuda, A.; Nakamura, Y.; Osuka, A.; Kim, D. *J. Am. Chem. Soc.* **2007**, 129, 10080-10081; for CuTPP: (c) Morone, M.; Beverina, L.; Abbotto, A.; Silvestri, F.; Collini, E.; Ferrante, C.; Bozio, R.; Pagani, G.A. *Org. Lett.* **2006**, 8, 2719-2722.
(19) This conclusion is based on the assumption that the system is under diffusion control; it was confirmed by varying the scan rate and plotting the square root of the scan rate versus the intensity of the redox peak yielding a linear plot (cf. Figure S14).
(20) Goutermann, M. in *The Porphyrins*, Dolphin, D., Ed.; Academic: New York, 1978.
(21) Typical metal-free porphyrin lifetimes are on the order of nano seconds.
(22) The choice of the counter anions (OTf^-, BF_4^- or ClO_4^-) does not appear to affect significantly the properties of dication $\mathbf{1}^{2+}$.
(23) The radical cation form of "exTTF" quickly disproportionates in the same solvent: Guldi, G. M.; Sanchez, L.; Martin, N. *J. Phys. Chem. B* **2001**, 105, 7139-7144.
(24) (a) Shen, Y.; Ryde, U. *Chem. Eur. J.* **2005**, *11*, 1549. (b) Bain-Ackerman, M. J.; Lavallee, D. K. *Inorg. Chem.* **1979**, 18, 3358.
(25) Todres, Z. V. *Ion-Radical Organic Chemistry: Principles and Applications,* 2nd ed.*;* CRC Press: Boca Raton, 2009.
(26) Calculations reveal that the spin density on the nitrogen atoms of $\mathbf{H_2TTFP}^{\bullet+}$ is relatively delocalized. This is consistent with the absence of appreciable hyperfine coupling seen in the EPR spectrum.
(27) Frere, P.; Allain, M.; Elandaloussi, E. H.; Levillain, E.; Sauvage, F.-X.; Riou, A.; Roncali, J. *Chem.–Eur. J.* **2002**, *8*, 784-792.
(28) (a) Kawashima, Y.; Ohkubo, K.; Fukuzumi, S. *J. Phys. Chem. A* **2012**, *116*, 8942−8948. (b) Fukuzumi, S.; Ohkubo, K.; Kawashima, Y.; Kim, D. S.; Park, J. S.; Jana, A.; Lynch, V. M.; Kim, D.; Sessler, J. L. *J. Am. Chem. Soc*. **2011**, *133*, 15938−15941.
(29) Gaussian 09, Revision A.1, Frisch, M. J.; Trucks, G. W.; Schlegel, H. B.; Scuseria, G. E.; Robb, M. A.; Cheeseman, J. R.; Scalmani, G.; Barone, V.; Mennucci, B.; Peterson, G. A.; Nakatsuji, H.; Caricato, M.; Li, X.; Hratchian, H. P.; Izmaylov, A. F.; Bloino, J.; Zheng, G.; Sonnenberg, J. L.; Hada, M.; Ehara, M.; Toyota, K.; Fukuda, R.; Hasegawa, J.; Ishida, M.; Nakajima, T.; Honda, Y.; Kitao, O.; Nakai, H.; Vreven, T.; Montgomery, Jr., J. A.; Peralta, J. E.; Ogliaro, F.; Bearpark, M.; Heyd, J. J.; Brothers, E.; Kudin, K. N.; Staroverov, V. N.; Kobayashi, R.; Normand, J.; Raghavachari, K.; Rendell, A.; Burant, J. C.; Iyengar, S. S.; Tomasi, J.; Cossi, M.; Rega, N.; Millam, N. J.; Klene, M.; Knox, J. E.; Cross, J. B.; Bakken, V.; Adamo, C.; Jaramillo, J.; Gomperts, R.; Stratmann, R. E.; Yazyev, O.; Austin, A. J.; Cammi, R.; Pomelli, C.; Ochterski, J. W.; Martin, R. L.; Morokuma, K.; Zakrzewski, V. G.; Voth, G. A.; Salvador, P.; Dannenberg, J. J.; Dapprich, S.; Daniels, A. D.; Farkas, Ö.; Foresman, J. B.; Ortiz, J. V.; Cioslowski, J.; Fox, D. J. Gaussian, Inc., Wallingford CT, **2009**.
(30) (a) Becke, A. D. *Phys. Rev. A* **1988**, 38, 3098. (b) Lee, C.; Yang, W.; Parr, R. G. *Phys. Rev. B* **1988**, *37*, 785.
(31) Yanai, T.; Tew, D.; Handy, N. *Chem. Phys. Lett*. **2004**, *393*, 51−57.
(32) Lahaye, D.; Muthukumaran, K.; Hung, C-H.; Gryko, D; Reboucas, J. S.; Spasojevic, I.; Batinic-Haberle, I.; Lindsey, J. S. *Bioorg. Med. Chem*. **2007**, *15*, 7066-6086.
(33) Steimecke, G.; Sieler, H. J.; Kirmse, R.; Hoyer, E. *Phosphorus Sulfur* **1979**, *7*, 49-55. (b) Simonsen, K. B.; Svenstrup, N.; Lau,

J.; Simonsen, O.; Mork, P.; Kristensen, G. J.; Becher, J. *Synthesis* **1996**, 407-418.
(34) Crystal Clear 1.40 (2008). Rigaku Americas Corporation, The Woodlands, TX.
(35) SIR97. A program for crystal structure solution. Altomare, A., Burla, M. C., Camalli, M., Cascarano, G. L., Giacovazzo, C., Guagliardi, A., Moliterni, A. G. G., Polidori, G. and Spagna, R. *J. Appl. Cryst*. **1999**, 32, 115-119.
(36) Sheldrick, G. M. SHELXL97. Program for the Refinement of Crystal Structures. *Acta Cryst*. **2008**, *A64*, 112-122
(37) Sluis, P. v. d.; Spek, A. L. SQUEEZE. *Acta Cryst*. **1990**, *A46*, 194-201.
(38) Spek, A. L (1998). PLATON, A Multipurpose Crystallographic Tool. Utrecht University, The Netherlands.
(39) WinGX 1.64. An Integrated System of Windows Programs for the Solution, Refinement and Analysis of Single Crystal X-ray Diffraction Data. Farrugia, L. J. *J. Appl. Cryst*. **1999**, *32*. 837-838.
(40) $R_w(F^2) = \{\Sigma_w(|F_o|^2 - |F_c|^2)^2 / \Sigma_w(|F_o|)^4\}^{1/2}$ where w is the weight given each reflection. $R(F) = \Sigma(|F_o| - |F_c|) / \Sigma(|F_o|)$ for reflections with $F_o > 4(\sigma(F_o))$. $S = [\Sigma_w((|F_o|^2 - |F_c|^2)^2 / (n - p)]^{1/2}$, where n is the number of reflections and p is the number of refined parameters.
(41) International Tables for X-ray Crystallography (1992). Vol. C, Tables 4.2.6.8 and 6.1.1.4, A. J. C. Wilson, editor, Boston: Kluwer Academic Press.
(42) Sheldrick, G. M. (1994). SHELXTL/PC (Version 5.03). Siemens Analytical X-ray Instruments, Inc., Madison, Wisconsin, USA.

TOC

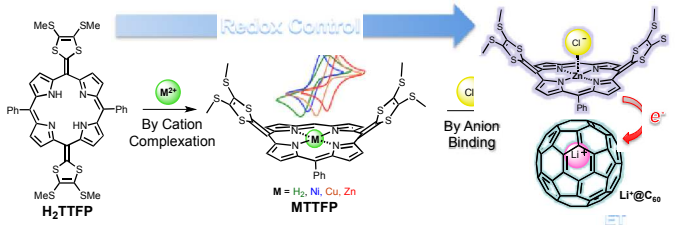
Redox Control
By Cation Complexation
By Anion Binding
H_2TTFP
M = H_2, Ni, Cu, Zn
MTTFP
$Li^+@C_{60}$